SEISMIC SOURCE CHARACTERIZATION AND ENERGY PARTITIONING FROM IN-MINE AND REGIONAL BROADBAND DATA IN SOUTH AFRICA

Eliza B. Richardson[1], Andrew A. Nyblade[1], William R. Walter[2], Kevin Mayeda[2], and Lindsay Lowe[2]

Penn State University[1] and Lawrence Livermore National Laboratory[2]

Sponsored by National Nuclear Security Administration
Office of Nonproliferation Research and Engineering
Office of Defense Nuclear Nonproliferation

Contract Nos. DE-FC03-02SF22673[1] and W-7405-ENG-48[2]

ABSTRACT

Mining-induced seismicity provides an important link between man-made and natural tectonic processes because it includes both fresh-fracturing events that are directly triggered by excavation and blasting, as well as events dominated by frictional slip which are analogous to tectonic earthquakes. These two types of events have distinguishable characteristics, such as different spatio-temporal clustering patterns, as well as different spectral signatures. Some previous studies using local in-mine data indicated that the fresh-fracturing events often have isotropic (explosional) moment tensors. Being able to differentiate the two types of events at regional and teleseismic distances is important for seismic verification studies.

We are studying a dataset of M > 2.5 mining-induced events that occurred between 1997 and 1999 in the Far West Rand gold-mining region of South Africa, approximately 80 km southwest of Johannesburg. The depth range of these events is 1.5 - 4 km; they were recorded locally by five networks of 109 three-component geophones installed at depth throughout the active mining environment. These events were also recorded at regional distances by a two-year PASSCAL deployment of 80 broadband stations.

Using a spectral method, we have calculated source parameters for these events from the in-mine recordings, including seismic moment, stress drop, corner frequency and energy. Larger stress drops are found than for frictional events, although the latter generally have larger seismic moments. S/P wave amplitude ratios are lower for fracturing events as well, which can be an indication of isotropic components of the source. From spectral analysis, scaling relations, and statistical analysis of the characteristic length scales between sequential frictional events, we confirm earlier estimates of the critical slip length (D_c ~ 100 microns) and critical patch size (R_c ~ 10 m). We believe these dimensions represent the nucleation size of events in this hard-rock mine environment.

We have inverted for the moment tensors of 15 events from the Far West Rand gold-mining region of South Africa that range in size from 1.0 < M < 3.2. These events occurred at 1-4 km depth and were recorded locally by four networks of 102 three-component geophones installed at depth throughout the active mining region as well as by a two-year PASSCAL deployment of 80 broadband seismometers. The moment tensors of the 15 events are consistent with purely double-couple solutions. In addition, we studied several events in the range 1 < M < 2 whose poor signal-to-noise ratio on the regional recordings prevented reliable moment tensor inversions. We presume that these events also have double-couple mechanisms based on their similar P/S amplitude ratios in comparison to the 15 well-characterized events. Therefore, we find little evidence in our data for seismic events with isotropic (explosional) mechanisms, at least down to the M = 1 level.

The broad southern Africa region offers the opportunity to examine variability in regional phase discriminants, such as high frequency P/S, which may be caused by unusually shallow depth events. We used a set of larger events (M>3.5) throughout the region to determine average source characteristics for the region and attenuation characteristics for each of the regional phases (Pn, Pg, Sn and Lg). We also determined moment magnitudes for these events using regional seismic coda envelopes. After correcting for source and path effects we find large variation in 6-8 Hz P/S ratio values (Pn/Lg, Pg/Lg and Pn/Sn). We are studying the behavior of these P/S values in terms of depth and focal mechanism effects.

OBJECTIVES

Mining-induced seismicity not only occurs at scales between those in the laboratory and those on tectonic faults, but can be recorded at the depth of seismic nucleation using in-mine seismometers, thus creating an excellent "natural laboratory" in which to study the physics of earthquake rupture. At present most gold mines in the Witwatersrand basin of South Africa use sophisticated underground arrays of geophones and accelerometers to record over 1,000 events per day. The extensive seismicity recorded at moment magnitude $M_w > 2$ provides a unique dataset to develop and test methods of discrimination between natural seismicity, mining tremors, and other industrially-related events such as chemical explosions. These $M_w > 2$ mining-induced events are large enough to be recorded on the in-mine arrays, as well as regionally by broadband seismometers. Therefore, locations, magnitudes, and focal mechanisms may be accurately determined from the high-frequency local data while regional phase propagation and energy partitioning may be studied via regional recordings. Another feature of this dataset is the variety of focal mechanisms as some mine events are purely double-couple shearing events whereas others have significant isotropic components (McGarr, 1992).

As the mines develop the technology to remove ore from deeper and deeper within the crust, larger stresses accumulate, producing higher rates of seismicity. Characterization of these events in terms of comparisons to other types of seismicity, both natural and man-made is important for building a comprehensive knowledge base of crustal seismic activity as well as for the pure science of earthquake physics and nucleation. In this study we seek to determine seismic source characteristics as well as moment tensors for a variety of mining-induced events in order to construct a catalog of "typical" large mining-induced events that can be used for source discrimination purposes as well as energy partitioning studies of the southern African crust.

RESEARCH ACCOMPLISHED

Source parameters

We have assembled a dataset of large ($M_w > 1.4$) mining-induced events from four gold mines in the Far West Rand region. The locations of these events were determined by operators at the mines via a ray-tracing algorithm based on body wave arrival times (Mendecki, 1993, 1997). This method incorporates a layered velocity model based on geologic units that have been determined by underground surveying and mapping as well as surface-based refraction profiles and borehole log data. The wavespeeds and location procedures have been verified by test blasting, so location uncertainties are typically on the order of 10-20 m for events of $M_w > 2$.

Using the spectral method developed by Andrews (1986) and adapted by Richardson & Jordan (2002) for use with in-mine seismic recordings, we have calculated source parameters for fourteen events that occurred in 1999, and 23 events from 1998 (see Table 1). Each of the events in this study were recorded by at least ten stations. In order to determine source parameters, we median-stacked each event's spectra and integrated the results up to the Nyquist frequency to determine S_D, the integral of the displacement power spectra (see Equation 6 of Andrews, 1986}), S_V, the integral of the velocity power spectra (see Equation 7 of Andrews, 1986), and A^2, the acceleration power spectral level (see Equation 19 of Andrews, 1986). These are used to determine the source parameters radiated energy (E), seismic moment (M_0) , and static stress drop ($\Delta\sigma$) as follows:

$$E = 4\pi\rho v S_V \tag{1}$$

$$M_0 = \frac{8\pi\rho v^3 S_D^{(3/4)}}{\Re S_V^{(1/4)}} \tag{2}$$

$$\Delta\sigma = \frac{2\pi f_0 \rho A^2}{C\Re} \tag{3}$$

in which the corner frequency is found by

$$f_0 = \left(\sqrt{S_V / S_D}\right) / 2\pi. \tag{4}$$

In the previous equations, ρ is the rock density, which has been determined experimentally at the mines, v is wavespeed, $\Re$ is a constant based radiation pattern, and C is also a small constant. An advantage of this method is that the exponent of the spectral rolloff is not a fixed parameter as in the case of fitting spectra with a Brune-type curve. Because our data is band-limited, there is an upper limit to the radiated energy we can determine (Ide & Beroza, 2001). However, in practice the underestimation of energy for this dataset is very small (approximately 5%) since typical corner frequencies for the events in this study are generally 1/5 to 1/10 of the Nyquist frequency (Richardson & Jordan, 2002).

In the following table, event dates and times are listed as yyyymmddhhmmss (The event times are local to the mines. Subtract two hours to get GMT time). Event locations are given by their latitude (°N), longitude (°E), and depth (meters below datum). It should be noted that event depths are referenced to the origin or "datum" of the Z axis of the local mine coordinates. This datum is a reference point in Johannesburg, and is 250 m above ground level and about 1800 m above sea level in the Carletonville Mining District where these events occurred (Figure 1). Seismic moment M_0 is in Nm, magnitude M_w is moment magnitude (Hanks & Kanamori, 1979), energy E is given in Joules, corner frequency f_0 is in Hz, and static stress drop $\Delta\sigma$ is in MPa.

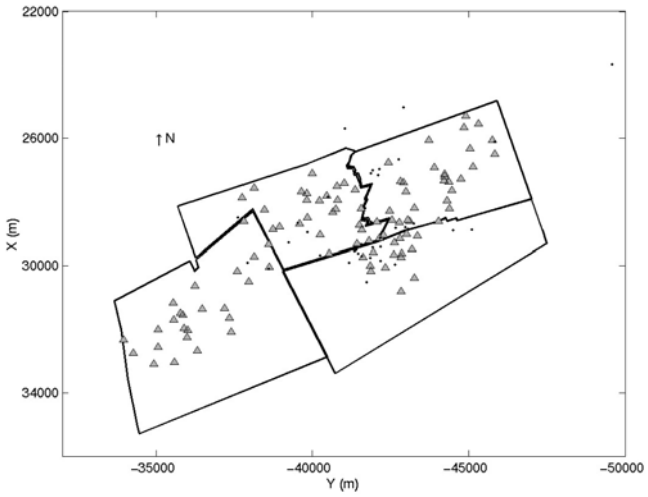

Figure 1. Map view of the lease areas of four mines in the Carletonville district (in mine coordinates). There are 102 three-component stations installed at depth (triangles). Dots represent the epicenters of large mining-induced events for which spectral source parameters were calculated (see Table 1) in this study.

Table 1. Source parameters of mining-induced events determined by in-mine array data. Events in bold are those for which moment tensors have been determined.

Event	Lat	Lon	Depth	M_0	M_w	E	f_0	$\Delta\sigma$
19980111144841	-26.401	27.411	2338	1.4e13	2.7	5.5e8	15.8	5.87
19980220050356	-26.429	27.430	3694	7.8e13	3.2	1.0e10	12.9	20.00
19980328134551	-26.437	27.417	2729	1.2e13	2.7	2.8e8	16.6	3.65
19980329051801	-26.435	27.422	2587	2.2e13	2.8	4.9e8	16.3	3.46
19980331135629	-26.439	27.380	2053	2.2e13	2.8	2.1e8	9.3	1.47
19980404190603	-26.430	27.399	2047	1.1e13	2.7	1.8e8	14.6	2.51
19980420170707	-26.395	27.430	2273	2.8e13	2.9	1.6e9	13.8	8.76
19980420194749	-26.412	27.422	1925	2.5e13	2.9	9.1e8	14.8	5.72
19980502123739	-26.414	27.419	1955	2.2e13	2.8	4.9e8	11.9	3.43
19980508103233	-26.440	27.427	2661	1.1e13	2.6	1.8e8	12.1	2.46
19980622162025	-26.439	27.423	2588	1.3e13	2.7	3.4e8	15.2	4.01
19980708212049	-26.434	27.416	2553	1.2e13	2.7	3.9e8	14.8	4.83
19980727135740	-26.427	27.419	2409	2.5e13	2.9	4.3e8	9.5	2.73
19981002194336	-26.432	27.423	2569	1.0e13	2.6	1.3e8	10.2	1.90
19981007192539	-26.420	27.406	3123	2.0e13	2.8	1.3e9	16.9	10.30
19981019200410	-26.436	27.416	2505	1.3e13	2.7	2.0e8	10.5	2.40
19981021044841	-26.434	27.420	2613	1.0e13	2.6	1.3e8	11.5	2.00
19981023160058	-26.437	27.420	2745	3.1e13	2.9	7.1e8	8.7	3.50
19981027090946	-26.426	27.377	2989	1.2e13	2.7	3.6e8	15.2	4.72
19981102163835	-26.427	27.434	2552	2.5e13	2.9	6.2e8	10.4	3.90
19981110172424	-26.404	27.459	2770	1.2e13	2.7	3.1e8	15.0	4.10
19981119170822	-26.414	27.422	2268	1.1e13	2.6	3.0e8	13.3	4.20
19981223093859	-26.433	27.393	3375	2.8e13	2.9	1.1e9	12.8	5.94
19990103155836	**-26.412**	**27.420**	**1748**	**1.1e13**	**2.6**	**1.2e7**	**12.1**	**0.87**
19990118102526	**-26.420**	**27.446**	**3422**	**9.0e11**	**1.9**	**9.4e6**	**27.3**	**0.80**
19990118112405	**-26.420**	**27.446**	**3443**	**2.0e11**	**1.4**	**1.1e6**	**36.1**	**0.68**
19990118200717	**-26.415**	**27.422**	**2039**	**2.9e12**	**2.2**	**1.9e7**	**15.9**	**0.51**
19990118213352	**-26.409**	**27.429**	**2879**	**9.1e12**	**2.6**	**1.6e7**	**15.0**	**1.00**
19990201194832	**-26.428**	**27.406**	**3137**	**4.8e12**	**2.4**	**3.4e7**	**13.6**	**0.53**
19990202123021	**-26.435**	**27.415**	**2582**	**1.2e13**	**2.7**	**3.2e7**	**13.6**	**3.00**
19990203221201	**-26.423**	**27.363**	**2638**	**1.4e12**	**2.0**	**1.5e7**	**23.4**	**1.98**
19990205025535	**-26.420**	**27.417**	**2991**	**4.3e12**	**2.3**	**5.8e7**	**17.6**	**1.37**
19990205175933	**-26.420**	**27.363**	**2686**	**3.1e11**	**1.6**	**5.0e6**	**44.3**	**3.07**
19990205205457	**-26.463**	**27.362**	**2558**	**2.9e12**	**2.2**	**3.1e7**	**18.5**	**0.96**
19990209154922	-26.477	27.329	2738	6.6e11	1.8	3.1e5	10.7	0.19
19990209195821	**-26.401**	**27.418**	**1618**	**4.2e13**	**3.0**	**9.2e8**	**9.3**	**3.20**
19990216053511	**-26.429**	**27.432**	**3761**	**1.2e13**	**2.7**	**9.2e6**	**10.4**	**0.56**
19990226143150	**-26.397**	**27.387**	**1981**	**4.5e12**	**2.4**	**2.2e6**	**12.3**	**0.53**
19990309161938	-26.435	27.415	2464	1.1e13	2.6	6.8e7	8.1	0.99
19990310023001	-26.429	27.428	2651	1.0e13	2.6	1.7e8	14.9	2.50
19990318193538	-26.428	27.396	395	4.6e13	3.1	1.5e9	11.5	5.20
19990703111216	-26.169	27.497	3099	2.2e13	2.9	1.8e8	18.5	10.60
19990709200228	-26.395	27.413	7235	5.5e13	3.1	9.7e8	8.7	4.00
19990718173016	-26.393	27.403	3823	7.0e13	3.2	1.2e9	8.6	4.80
19990907150924	-26.386	27.446	3634	4.0e13	3.0	2.7e9	13.0	10.90
19990923132820	-26.386	27.452	4028	4.1e13	3.0	1.5e9	13.3	10.30

Moment tensors of selected events

We determined moment tensors for events that covered a range of magnitudes, depths, and locations to provide as much variation as possible in composing a catalog of "typical" large mining-induced events. Some events are also part of foreshock-mainshock-aftershock sequences. We followed the method outlined in Ammon et al. (1998) and calculated regional Green's functions, then inverted for the moment tensors using broadband data from the Kaapvaal PASSCAL deployment. Since we used the PASSCAL data alone, we obtained independent measurements from those of the in-mine array data previously used to determine the source parameters (see Table 1). A comparison of event magnitudes as calculated by the spectral method using only the in-mine array data with magnitudes determined as part of the moment-tensor inversion is shown in Figure 3. By only using eight nearby stations for the inversions (see Figure 2), we will be able to use the more distant stations for regional phase amplitude analysis; therefore, the results of the two studies will be independent of each other.

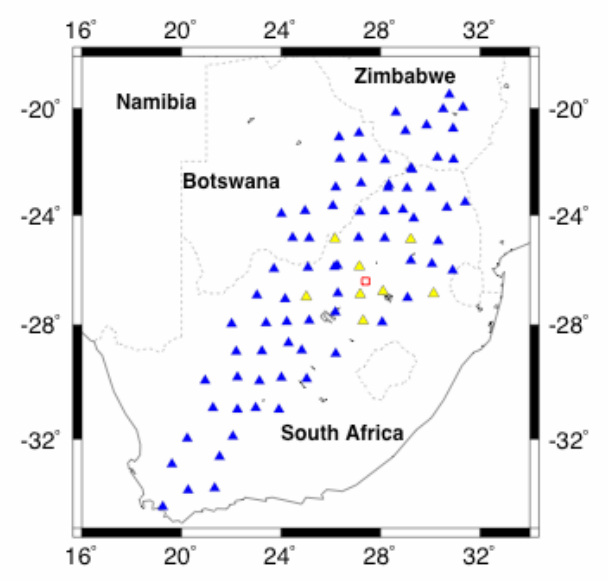

Figure 2. Map of southern Africa showing locations of the Kaapvaal Craton PASSCAL deployment (triangles). Yellow triangles are the stations used in the moment tensor inversions. The small red box is the area shown in detail in Figure 4.

To compute regional Green's functions, we used a simple 45-km thick crustal half-space for the velocity model based on the results of receiver function analysis of the crustal structure of the Archean craton by Nguuri et al. (2001). This study determined that crustal thickness ranged from approximately 41-50 km across the area covered by the stations used in our moment tensor inversions. We used wavespeed and density values determined experimentally by the mines (P = 6.1 km/s, S = 3.65 km/s, $\rho = 2.7 g/cm^3$).

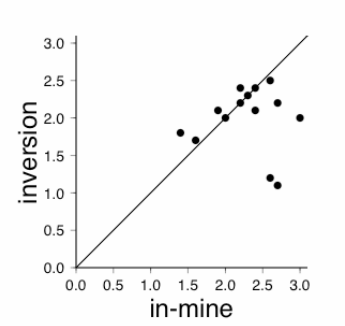

Figure 3. Comparison between moment magnitude as determined by the spectral analysis using in-mine seismic data and that determined through the moment tensor inversion using the broadband data. The 1:1 line is drawn for reference.

The results of the moment tensor inversions are given in Table 2. These are fully deviatoric tensors. We allowed the moment tensors to have some isotropic component in the inversion, but none were significantly isotropic. It has been shown that S/P-wave amplitude ratios of mining-induced events are often smaller for events with significant isotropic components when compared with purely double-couple events of approximately the same moment (Cichowicz et al., 1990; Gibowicz et al., 1991). Therefore, using the in-mine recordings, we calculated high-frequency (> 10 Hz) S/P-wave amplitude ratios of several other events between $1 < M_w < 2$ whose signal-to-noise ratios were not good enough to perform moment tensor inversions using broadband data. The S/P-wave amplitude ratios were not significantly different than those of the double-couple events for which we determined moment tensors, and therefore we do not expect significant isotropic components of the source down to at least $M_w = 1$. It should be noted that the previous studies involving S/P-wave amplitude ratios were conducted with events of $M_w < 0$.

The fourteen events for which we determined moment tensors ranged in size from $1.4 < M_w < 3.0$ and ranged in depth from 1.6 km to 3.8 km. This depth range is typical of the larger mining-induced events in the Carletonville district. We do not observe any significant trend in type of faulting with either depth or event size (see Figure 4). The events in this study so far show two major modes of failure: normal faulting and strike-slip faulting. It is surprising to find such a large population of strike-slip events in this group, as the vast majority of faults observed underground have measurable offsets consistent with normal motion alone. There are several possibilities for this apparent discrepancy. Not all seismogenic faults are directly visible underground, therefore there may be an historical bias in favor of normal faults because of observational limitations. In addition, the faults observed underground have yet to be studied in detail to determine whether all fault offset is due to seismic activity, or whether there is some creep. For example, do faults creep in a normal sense, but release seismic energy in a strike-slip or dip-slip pattern? Strike-slip motion is inherently difficult to discern when there is only limited visible access and when the displacement is not large enough to juxtapose different formations. There has been little in the way of detailed analysis of fault cores taken from depth; therefore sense of motion has been assumed, but may in fact be a relic of ancient fault activity that predates the active mining. It may also be that these moment tensors, which were determined by surface broadband data alone are not accurate, although the waveform fits are generally good. An obvious next step in this analysis will be to perform a joint inversion using in-mine data for moment tensor analysis. In addition, S-wave data could be included in the moment-tensor inversions.

Table 2. Moment tensors of mining-induced events

Event	M_{xx}	M_{xy}	M_{xz}	M_{yy}	M_{yz}	M_{zz}
19990103155836	-0.273E-03	-0.268E-02	0.230E-02	-0.583E-02	0.222E-02	0.611E-02
19990118102526	0.623E+00	-0.121E+01	0.179E-01	-0.152E+01	0.552E+00	0.896E+00
19990118112405	0.832E+00	-0.275E+01	-0.352E-02	-0.166E+01	-0.306E+00	0.828E+00
19990118200717	-0.132E+01	-0.169E+01	0.256E-01	0.239E+01	-0.965E-01	-0.107E+01
19990118213352	-0.382E+00	-0.185E+00	-0.166E-01	0.616E+00	-0.406E+00	-0.233E+00
19990201194832	0.186E -01	0.151E+00	-0.140E+00	0.112E+00	-0.273E+00	-0.131E+00
19990202123021	-0.118E+00	-0.320E-01	-0.143E-01	0.275E+00	-0.193E-01	-0.157E+00
19990203221201	-0.188E+01	-0.154E+01	-0.125E-01	0.363E+01	0.884E-01	-0.175E+01
19990205025535	0.135E+01	0.194E+01	-0.961E-01	-0.240E+01	0.309E+00	0.106E+01
19990205175933	0.738E+00	-0.674E+00	-0.229E-01	-0.123E+01	0.135E+00	0.496E+00
19990205205457	0.408E+00	0.895E+00	-0.760E-01	-0.965E+00	0.318E+00	0.557E+00
19990209154922	-0.610E+00	-0.143E+01	0.560E-01	0.121E+01	-0.242E+00	-0.603E+00
19990216053511	0.353E-02	-0.130E-02	-0.270E-02	-0.360E-02	0.155E-02	0.738E-04
19990226143150	0.406E-02	-0.919E+00	-0.456E-01	0.190E+00	0.275E+00	-0.194E+00

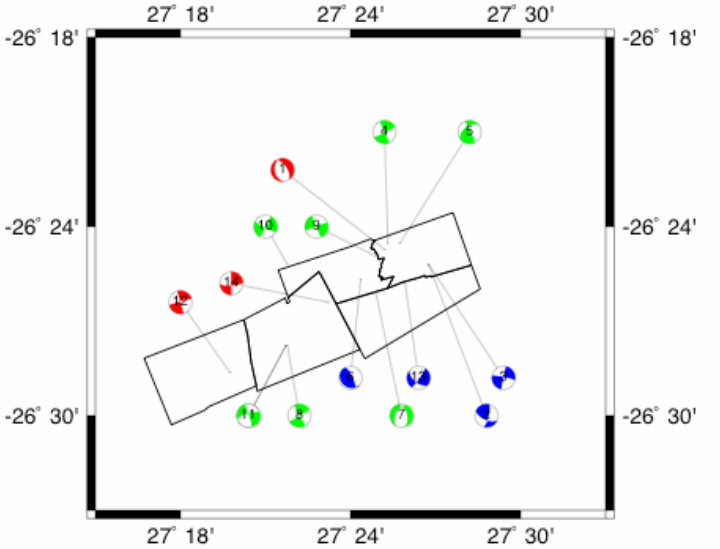

Figure 4. Map view of the lease areas of five mines in the Carletonville district with locations and focal mechanism (FC) diagrams of the events for which moment tensors have been determined. Events are labeled in chronological order (The FC labeled "1" is 19990103155836, and the FC labeled "14" is 19990226143150, etc.). Red FCs denote events whose depths are between 1-2 km, green FCs are for events between 2-3 km and blue FCs show events whose depths are between 3-4 km.

Regional P/S amplitude measurements

In order to obtain geometric spreading, attenuation and coda amplitude corrections for the permanent International Monitoring Station (IMS) stations in southern Africa (BOSA, LBTB, SUR), we picked Pn, Pg, Sn, and Lg arrivals for all events of M > 2.5 in the Lawrence Livermore National Laboratory (LLNL) database from 1998 – 2004. We then culled this dataset to events of M > 3.5 to perform the station calibrations. We determined coda M_w for these events as well based on the well-studied large event of October 30, 1994 (e.g. Bowers, 1997). The locations of these M > 3.5 events are shown in Figure 5.

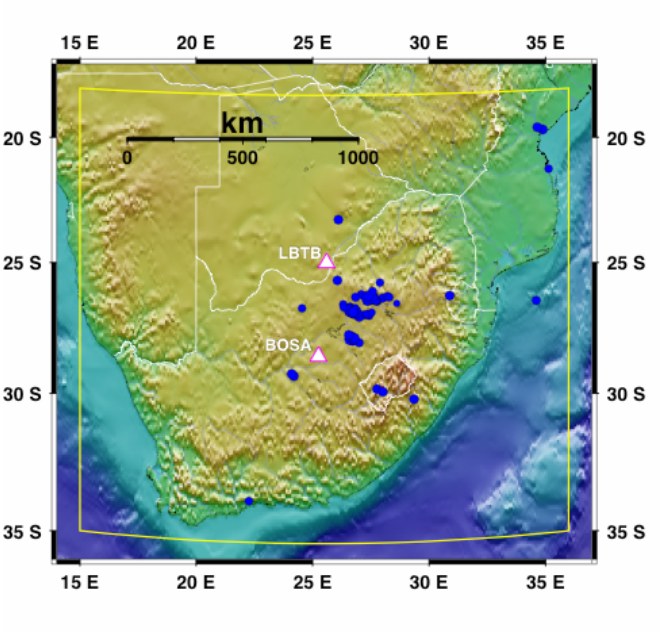

Figure 5. Map of southern Africa showing the location of M > 3.5 events (blue circles) used to determine regional geometric spreading, attenuation, and coda amplitudes for comparison with the target events in our database. Permanent stations BOSA and LBTB are white triangles.

We next used the coda M_w's for these events to remove distance and magnitude trends from the high frequency discrimination amplitude ratios (see Figure 6). This dataset spans a narrow range of frequency and magnitude, so no trend is readily apparent in the raw measurements of amplitude ratios with respect to magnitude (compare the bottom two plots in each set of quad plots in Figure 6). The magnitude and distance amplitude correction (MDAC) removes the significant trend with respect to source-receiver distance (compare the top two plots in each set of quad plots in Figure 6) in the amplitude ratios at this frequency band.

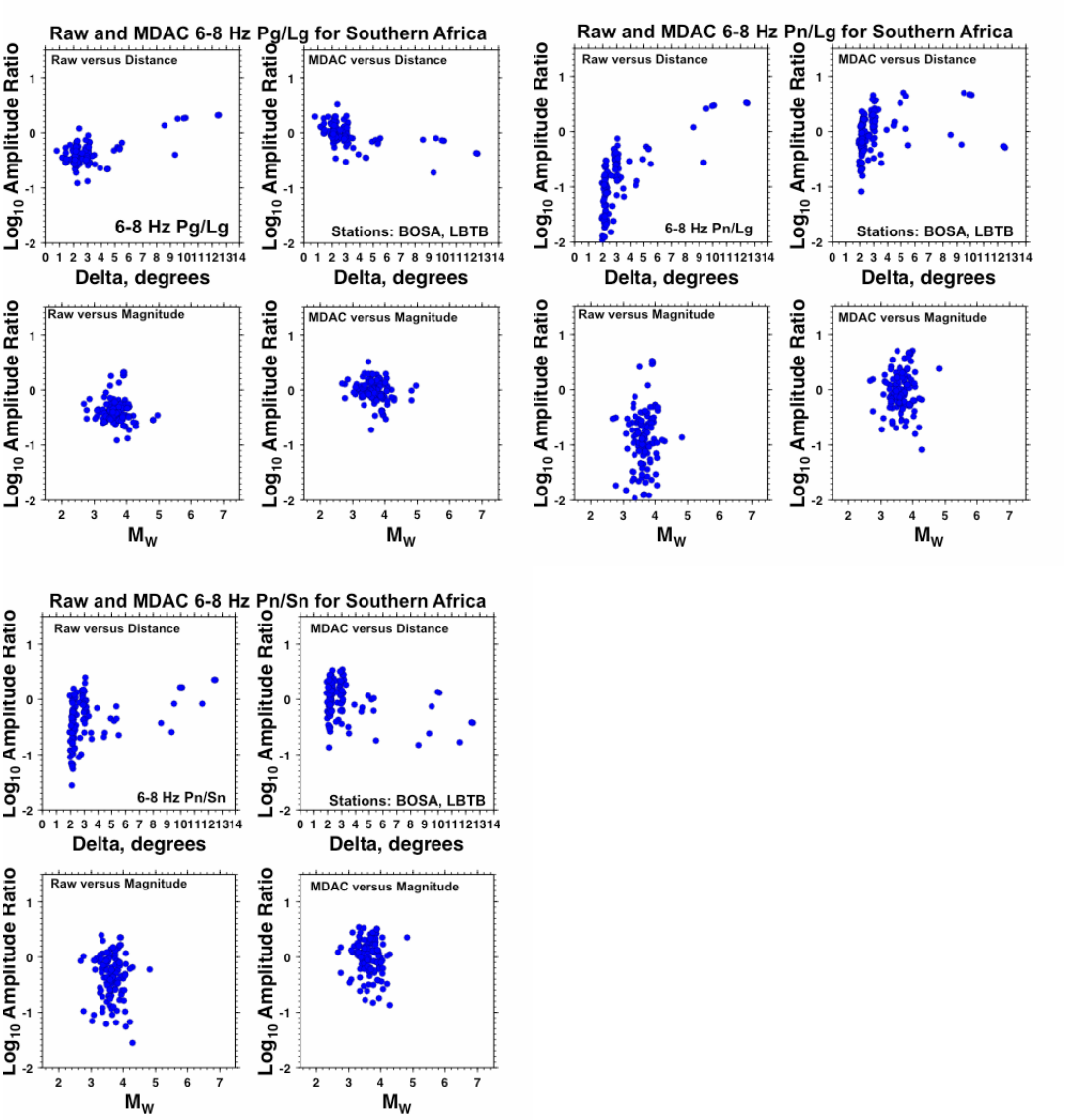

Figure 6. Regional P/S amplitude ratios at 6-8 Hz for the events in Figure 5. Each set of quad plots shows raw measurements (left) and measurements whose amplitudes have been corrected for magnitude and distance (right) for a given amplitude ratio as a function of source-receiver distance (top) and as a function of magnitude (bottom). The first set of quad plots is for the ratio Pg/Lg, the second is for the ratio Pn/Lg, and the third is for Pn/Sn.

Many prior studies have shown that high frequency P/S ratios have the potential to discriminate earthquakes from explosions (e.g., Walter et al. 1995, Battone et al. 2002), particularly after correcting for source and path effects (e.g., Taylor et al. 2002). The range of high frequency P/S values in Figure 6 is fairly large, even after correcting for source and path effects. We want to understand the source of this variability and suspect that some of it comes from the presence of mine-related seismicity, which has very shallow depths and potentially a greater range in focal mechanism, as compared with ordinary tectonic events. To examine the effects of depth and mechanism on P/S ratios and other regional discriminants, we plan to determine the regional phase amplitudes of the mine-related events in Table 1, and Table 2 where depth and focal mechanism, respectively, have been independently determined. We will estimate the coda moment magnitudes and use the source and path corrections as determined from the larger background events shown in figures 5 and 6. We also plan to determine some additional depths and focal mechanisms for a few of the larger events shown in Figure 5 that are amenable to regional waveform modeling.

CONCLUSIONS AND RECOMMENDATIONS

We have calculated source parameters for 46 mining-induced events of $M_w > 1$ and inverted for the best-fitting moment tensors for 14 events and do not find any significant isotropic components of the source for any of the events studied. This supports the hypothesis that large mining-induced failures occur by shearing of pre-existing planes of weakness under frictionally-controlled conditions (i.e., high normal stress) and that these events are physically analogous to natural tectonic earthquakes. A surprising number of strike-slip mechanisms were determined, in contrast to normal faulting, which was expected. There have been few thorough studies of the source characteristics of these events to date with which to compare our results. Therefore, we must continue to determine more moment tensors, and we must incorporate the in-mine data in a joint inversion for the moment tensors. The next step in the characterization of these mining-induced events is to take the ground-truthed depth and mechanism data and combine this with the MDAC-corrected data to look for depth and focal mechanism trends. We also plan to determine more accurate locations and mechanisms for some of the larger tectonic events in the LLNL database so that we will obtain two separate datasets whose origins are known (tectonic and mining-related).

ACKNOWLEDGEMENTS

We thank Chuck Ammon for lending us his expertise in calculating local and regional Green's functions.

REFERENCES

Ammon, C. J., R. B. Herrmann, C. A. Langston and H. Benz (1998), Source parameters of the January 16, 1994 Wyomissing Hills, Pennsylvania earthquakes, *Seism. Res. Letters* 69: 261-269.

Andrews, D. J. (1986), Objective determination of seismic source parameters and similarity of earthquakes of different size, in *Earthquake Source Mechanics*, S. Das, J. Boatwright, C.H. Scholz, eds, vol. 6 of Geophysical Monograph *Am. Geophys. Union* 37: 259-267.

Battone, S., M. D. Fisk and G. D. McCarter (2002), Regional Seismic-Event Characterization Using a Bayesian Formulation of Simple Kriging, *Bull. Seism. Soc. Am*. 92: 2277-2296.

Bowers, D. (1997), The October 30, 1994 seismic disturbance in South Africa: Earthquake or large rockburst?, *J. Geophys. Res*. 102: 9843-9857.

Cichowicz, A., R. W. E. Green, A. van Zyl Brink, P. Grobler and P. I. Mountfort (1990), The space and time variation of micro-event parameters occurring in front of an active stope, in *Rockbursts and Seismicity in Mines*, ed. C. Fairhurst, 2: 171-175.

Gibowicz, S. J., R. P. Young, S. Talebi, and D. J. Rawlence (1991), Source parameters of seismic events at the Underground Research Laboratory in Manitoba, Canada: Scaling relations for events with moment magnitude smaller than –2, *Bull. Seism. Soc. Am*. 81: 1157-1182.

Hanks, T.C. and H. Kanamori (1979), A moment magnitude scale, *J. Geophys. Res*. 84: 2348-2350.

Ide, S. and G. C. Beroza (2001), Does apparent stress vary with earthquake size?, *Geophys. Res. Lett.* 28**:** 3349-3352.

Mendecki, A. J., ed., *Seismic Monitoring in Mines*, Chapman and Hall, 1997.

Mendecki, A. J. (1993), Real time quantitative seismology in mines, Keynote lecture in *Proceedings of the 3rd International Symposium on Rockbursts and Seismicity in Mines*, ed. By R. P. Young, Balkema, Rotterdam, pp. 1141-1144.

McGarr, A. (1992), Moment tensors of ten Witwatersrand mine tremors, *Pure Appl. Geophys.* 139**:** 781-800.

Nguuri, T. K., J. Gore, D. E. James, S. J. Webb, C. Wright, T. G. Zengeni, O. Gwavava, J. A. Snoke, and Kaapvaal Seismic Group (2001), Crustal structure beneath southern Africa and its implications for the formation and evolution of the Kaapvaal and Zimbabwe cratons, *Geophys. Res. Lett*. 28, pp. 2501-2504.

Richardson, E. and T.H. Jordan (2002), Seismicity in deep gold mines of South Africa: Implications for tectonic earthquakes, *Bull. Seism. Soc. Am*. 92, pp. 1766-1782.

Taylor, S., A. Velasco, H. Hartse, W. S. Philips, W. R. Walter, and A. Rodgers, (2002). Amplitude corrections for regional discrimination, *Pure. App. Geophys*. 159, 623-650.

Walter, W. R., K. Mayeda, and H. J. Patton (1995), Phase and spectral ratio discrimination between NTS earthquakes and explosions Part 1: Empirical observations, *Bull. Seism. Soc. Am.* 85, 1050-1067.